Environmental Science & Technology

pubs.acs.org/est

Article

Spaceborne Observations of Lightning NO_2 in the Arctic

Xin Zhang,* Ronald van der A, Jieying Ding, Henk Eskes, Jos van Geffen, Yan Yin,* Juliëtte Anema, Chris Vagasky, Jeff L. Lapierre, and Xiang Kuang

Cite This: https://doi.org/10.1021/acs.est.2c07988

Read Online

ACCESS | Metrics & More | Article Recommendations | Supporting Information

ABSTRACT: The Arctic region is experiencing notable warming as well as more lightning. Lightning is the dominant source of upper tropospheric nitrogen oxides (NO_x), which are precursors for ozone and hydroxyl radicals. In this study, we combine the nitrogen dioxide (NO_2) observations from the TROPOspheric Monitoring Instrument (TROPOMI) with Vaisala Global Lightning Dataset 360 to evaluate lightning NO_2 (LNO_2) production in the Arctic. By analyzing consecutive TROPOMI NO_2 observations, we determine the lifetime and production efficiency of LNO_2 during the summers of 2019−2021. Our results show that the LNO_2 production efficiency over the ocean is ∼6 times higher than over continental regions. Additionally, we find that a higher LNO_2 production efficiency is often correlated with lower lightning rates. The summertime lightning NO_x emission in the Arctic (north of 70° N) is estimated to be 219 ± 116 Mg of N, which is equal to 5% of anthropogenic NO_x emissions. However, for the span of a few hours, the Arctic LNO_2 density can even be comparable to anthropogenic NO_2 emissions in the region. These new findings suggest that LNO_2 can play an important role in the upper-troposphere/lower-stratosphere atmospheric chemical processes in the Arctic, particularly during the summer.

KEYWORDS: *Arctic, lightning, nitrogen dioxide, satellite measurements, TROPOMI*

INTRODUCTION

Warming of the climate system is invoking changes in global lightning.[1−3] Many modeling schemes have been developed over the past 30 years to predict lightning.[4−9] Most climate models predict more lightning in the mid-latitudes,[9−12] but predictions for the tropics are currently diverging.[13,14] In the Arctic, where warming is 4 times faster than the global average, relatively few studies have been conducted.[15] Recently, Chen et al.[16] developed a lightning modeling scheme for the Arctic. Their study suggested a 74−150% increase in the rate of lightning in the permafrost region by the end of the century for a 3.7 °C global mean temperature increase. Ground-based lightning observations support this conclusion, showing that the relative fraction of Arctic lightning over global lightning has tripled from 2010 to 2020.[17] In addition, increased summer moisture convergence in the Arctic is expected to strengthen convective systems, leading to more lightning.[18]

Lightning produces nitrogen oxide (NO) through the dissociation of O_2 and N_2 at high temperatures.[19] NO is rapidly oxidized to nitrogen dioxide (NO_2), and an equilibrium is established between NO and NO_2. NO_2 can be detected by satellite, making it a useful tracer for studying lightning processes. Global lightning NO_x (LNO_x) emissions are estimated to be 5 ± 3 Tg of N $year^{-1}$ and are the dominant natural source of NO_x in the upper troposphere.[20] Lightning NO_2 (LNO_2) has a longer lifetime in the upper troposphere due to the colder temperature and lower reaction rate.[21,22] Its lifetime ranges from 2 to 12 h near the initial convection and increases to at least 2−3 days downwind of convection,[23] leading to more ozone (O_3) after several days.[24−26] O_3 is known as a significant greenhouse gas;[27] thus, LNO_x has an indirect effect on climate forcing. Furthermore, the photolysis of O_3 produces oxygen atoms in a higher-energy state, which react with water vapor to produce the hydroxyl radical (OH), an atmospheric oxidant. Greater LNO_x emissions shift the equilibrium between OH and HO_2 toward more OH.[28] Lightning also directly creates OH through the dissociation of H_2O by visible flashes and subvisible charges.[29−32] The increase in the level of OH will ultimately reduce the levels of carbon monoxide (CO) and methane (CH_4), another greenhouse gas.[33,34] Lightning can also trigger wildfires that emit carbon dioxide in the Arctic.[16] Therefore, a better understanding of Arctic LNO_x emissions is important for determining trace gas changes in the Arctic.

Received: October 28, 2022
Revised: January 25, 2023
Accepted: January 25, 2023

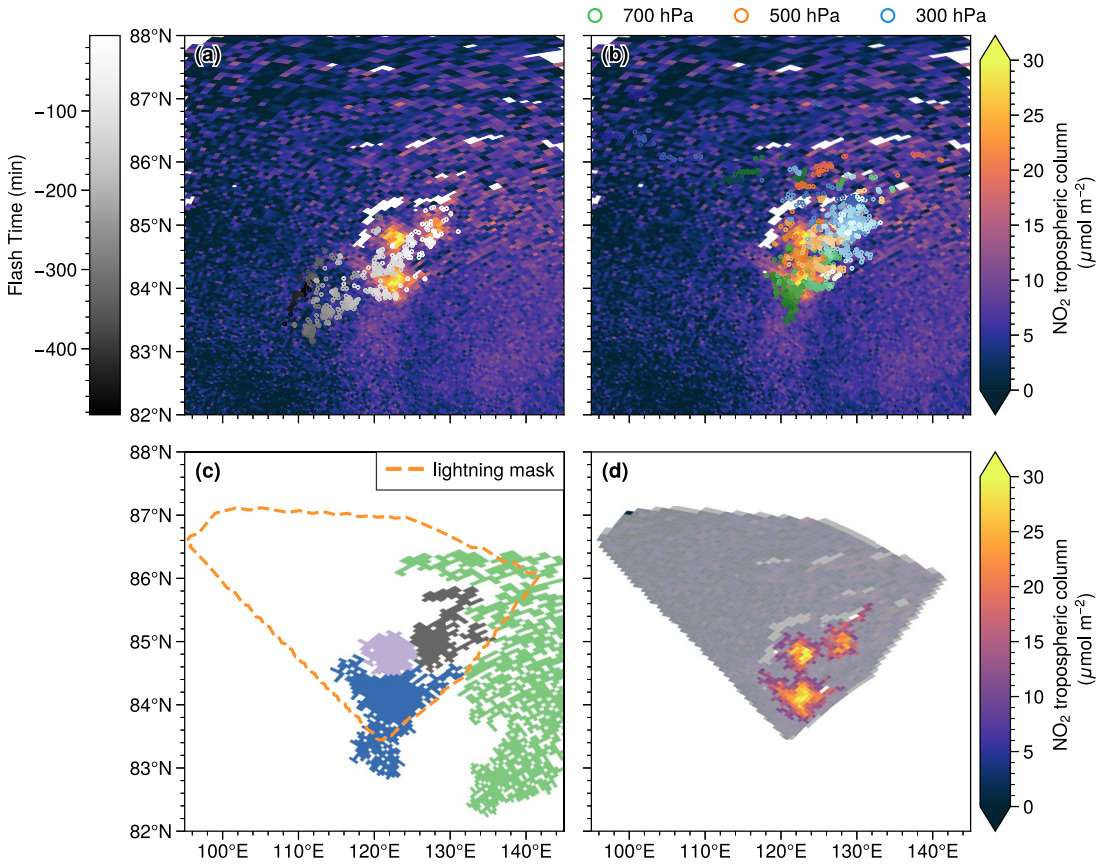

Figure 1. Overview of the process for identifying lightning NO_2 pixels from TROPOMI orbit 09458 on August 1, 2019. The TROPOMI-detected NO_2 tropospheric columns are overlaid with (a) observed lightning strokes and (b) transported air parcels of lightning NO_2 at three pressure levels [300 hPa (blue), 500 hPa (orange), and 700 hPa (green)]. (c) Parcels are combined into one lightning mask (orange circle), which overlaps with high NO_2 selections (filled pixels). The different pixel colors represent different NO_2 selections based on multiple NO_2 thresholds. (d) Final selection (bright colored pixels) of NO_2 tropospheric columns affected by lightning NO_2 within the mask.

Estimating LNO_x requires knowledge of lightning counts and the production efficiency (PE, NO_x per lightning). While there have been several studies on Arctic lightning counts,[16,17,35] the LNO_x PE for this region is not well quantified. Previous laboratory studies, as well as airborne and satellite-based observations, have estimated that the PE for individual flashes ranges from ≈5 to >1000 mol of NO_x.[20] It is uncertain whether mid-latitude lightning is more efficient at producing NO_x than tropical lightning. Some findings from individual storms suggest that this may be the case,[36−38] but recent satellite-based observations suggest little difference.[39,40] Considering the regional differences and limited work at the high latitudes, we focus on quantifying the LNO_2 PEs in the Arctic. In this study, we evaluate the NO_2 observations from the TROPOspheric Monitoring Instrument (TROPOMI) with lightning strokes detected by Vaisala Global Lightning Dataset 360 (GLD360). Using consecutive TROPOMI orbits, we are able to determine the LNO_2 lifetime and PEs in the Arctic for the first time, providing insight into regional differences in LNO_2 emissions.

DATA AND METHODOLOGY

Lightning Data. The GLD360 network has been in operation since 2009 and consists of very-low-frequency lightning detection sensors located around the world. These sensors can detect both cloud-to-ground (CG) and intracloud (IC) strokes.[41−43] The detection efficiencies of CG and IC strokes over the Arctic ocean are estimated to be 50−60% and <10%, respectively.[44] In the Arctic, the total number of lightning strokes is adjusted to be 4 times the number of detected strokes, on the basis of the constant ratio (≈1) of IC to CG strokes in this region. The constant ratio is calculated using two factors: the number of strokes per flash (flash multiplicity) and the mean ratio of IC to CG flashes (also known as the Z ratio) in the high latitudes. The flash multiplicity is highly sensitive to both the detection efficiency and the algorithm used to group strokes into flashes.[45−48] The mean multiplicity value for high-latitude studies is estimated to be 1.2.[49] In addition, the mean Z ratio of high-latitude flashes is between 1 and 1.3.[50−52] To evaluate the sensitivity of the constant ratio, we have used different values (1:2 and 2:1) in Table S4 to assess the uncertainty of estimated LNO_x emissions.

To evaluate the lightning distribution changes at high latitudes, we compare the lightning stroke data from the GLD360 data (2019−2021) with lightning flashes detected by the Optical Transient Detector (OTD, 1996−1999).[53] The OTD data product includes only the number of flashes, while one flash can contain one or more strokes. Because the official GLD360 product includes only lightning strokes and our purpose is to investigate changes in lightning distribution, we do not group strokes into flashes. The GLD360 data cover the entire high-latitude region (>60° N), while the OTD instrument observed lightning only south of 75° N. During

https://doi.org/10.1021/acs.est.2c07988
Environ. Sci. Technol. XXXX, XXX, XXX−XXX

the summer season (June−August), the fraction of GLD360 strokes occurring north of 75° N is 3% for the period of 2019−2021 (Figure S2).

NO_2 Satellite Measurements. The TROPOMI instrument is on board the Sentinel 5 Precursor (S5P) satellite, flying in a near-polar, sun-synchronous orbit.[54] The nadir pixel resolution has been enhanced from 7 × 3.5 to 5.5 × 3.5 km^2 since August 6, 2019. Its wide swath width (~2600 km) results in overlapping ground pixels for high latitudes. For example, a high-latitude site north of 70° N can have up to seven overpasses in summer, as the detection is also available during the descending orbit. This means that Arctic NO_2 can be tracked from space with an interval of 100 min, the period of a single orbit.

The TROPOMI NO_2 product is the S5P Product Algorithm Laboratory (S5P-PAL) reprocessing product, version 2.3.1, which has improved validity over bright storm scenes compared to earlier versions.[55] To minimize the impact of boundary layer NO_2 and improve the accuracy of estimating the background, we consider only observations north of 70° N, where the summertime average NO_2 column density is relatively low [<15 μmol m^{-2} (Figure 3a)]. We also exclude pixels with large retrieval errors (processing quality flags >0).

Estimation of Lightning NO_2. The LNO_2 estimation in this study involves three main steps: (1) identifying high NO_2 columns associated with lightning strokes using wind data, (2) calculating LNO_2 columns using a new algorithm, and (3) determining the LNO_2 production efficiency using consecutive TROPOMI observations.

Procedure for Lightning Clustering. We cluster lightning strokes within a 40 km radius of each stroke and a 12 h period[56] before the TROPOMI overpass time using the Density-Based Spatial Clustering of Applications with Noise (DBSCAN) algorithm.[57,58] Because wildfires can also produce NO_2, the lightning clusters affected by wildfire emissions are identified and filtered out using the Visible/Infrared Imager/Radiometer Suite (VIIRS) 375m active fire product. The VIIRS is on board the Suomi National Polar-orbiting Partnership (Suomi-NPP), which is in the same orbit but 3.5 min ahead of S5P. We refer to lightning clusters without fires inside as "clean" clusters.

For each clean lightning cluster, we define air parcels affected by LNO_2 at three pressure levels (300, 500, and 700 hPa) on the basis of the time and location of detected strokes (Figure 1a). The air parcels containing LNO_2 are then transported by horizontal advection (Figure 1b). To determine the location of air parcels at the TROPOMI overpass time, we use the hourly fifth generation of atmospheric reanalysis (ERA5) wind data.[59] The isobaric forward trajectories at the three pressure levels are used to construct an approximate LNO_2 region. The final locations of air parcels are combined into one lightning mask (the orange circle in Figure 1c), which is used to determine the background NO_2 and LNO_2 pixels.

In this study, we use a watershedding technique to derive the area of high NO_2 vertical column density (V_{NO_2}, pixels in Figure 1c). This method treats the pixel values as a topographic surface and separates them into individual regions known as catchment basins.[60,61] Threshold values ranging from 4×10^{14} to 1×10^{15} molecules cm^{-2} are applied in steps of 2×10^{14} molecules cm^{-2} to detect multiple localized high-NO_2 features. These features are used to identify nearby areas with high V_{NO_2} values (pixels of different colors in Figure 1c). Detailed steps of the watershedding process are described by Heikenfeld et al.[61] The lightning cluster containing one or more high-V_{NO_2} areas is selected for further analysis of LNO_2. The final LNO_2 area (bright colored pixels in Figure 1d) is the region with a high V_{NO_2} that is reidentified by the watershedding method within the lightning mask (see the Supporting Information for details).

Calculation of the Lightning NO_2 Vertical Column. As discussed by Zhang et al.,[28] the official TROPOMI algorithm does not include the LNO_2 in the NO_2 retrieval. Thus, we subtract the background NO_2 from the official S_{NO_2} and convert the difference to the tropospheric LNO_2 vertical column with an air mass factor (AMF). The algorithm is expressed as

$$V_{LNO_2} = \frac{S_{NO_2} - S_{BG}}{AMF_{LNO_2}} \quad (1)$$

where V_{LNO_2} is the tropospheric LNO_2 vertical column, S_{NO_2} is the TROPOMI-measured tropospheric NO_2 slant column, and AMF_{LNO_2} is a customized lightning air mass factor. Following Allen et al.,[56] the background S_{NO_2} (S_{BG}) is defined as the product of the tropospheric AMF and the 30th percentile of V_{NO_2} over low-NO_2 pixels within the lightning mask. The low-NO_2 region (gray pixels in Figure 1d) includes all masked pixels outside of the high-V_{NO_2} regions identified by the watershedding technique. AMF_{LNO_2} is the ratio of the "visible" LNO_2 slant column to the total tropospheric LNO_2 vertical column:

$$AMF_{LNO_2} = \frac{(1 - f_r)\int_{p_{surf}}^{p_{tp}} w_{clear}(p)\, LNO_2(p)\, dp + f_r \int_{p_{cloud}}^{p_{tp}} w_{cloudy}(p)\, LNO_2(p)\, dp}{\int_{p_{surf}}^{p_{tp}} LNO_2(p)\, dp} \quad (2)$$

where f_r is the cloud radiance fraction in the NO_2 window, p_{surf} is the surface pressure, p_{cloud} is the cloud pressure, p_{tp} is the tropopause pressure, w_{clear} and w_{cloudy} are the pressure-dependent scattering weights from the lookup table[62] for clear and cloudy parts, respectively, and $LNO_2(p)$ is a pressure-dependent tropospheric NO_2 profile presented by a modified Gaussian distribution. The peak width of the Gaussian distribution is set to 180 hPa following Ott et al.[63] and Luo et al.[64] (see the Supporting Information for details), and the peak level is the highest TROPOMI cloud pressure in the lightning mask.

The scattering weights used in the calculation of AMF_{LNO_2} are determined by five parameters: surface pressure, solar zenith angle, viewing zenith angle, relative azimuth angle, and albedo. For the cloudy part, the surface pressure and albedo values used in the lookup table are specific to the clouds present. The surface pressure is set equal to the cloud pressure, and the albedo is set equal to the cloud albedo. The cloud

https://doi.org/10.1021/acs.est.2c07988
Environ. Sci. Technol. XXXX, XXX, XXX−XXX

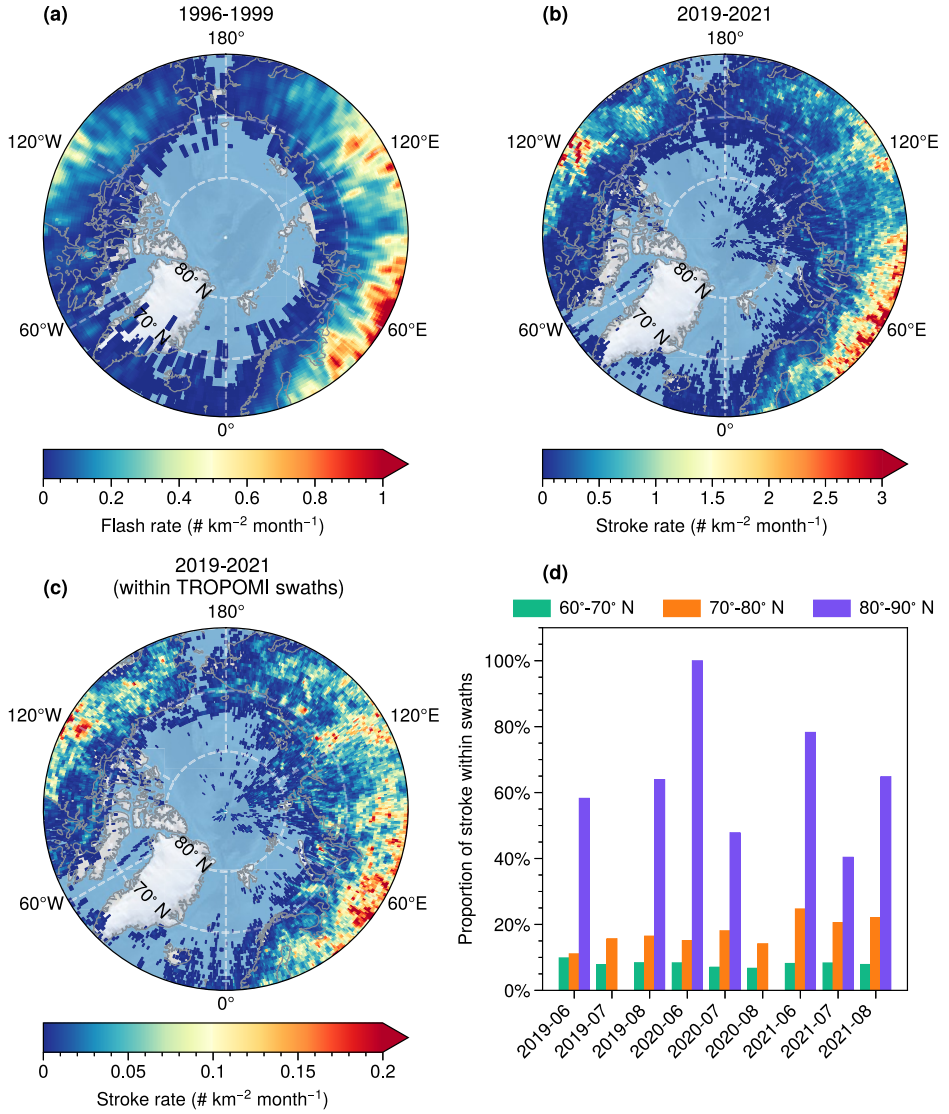

Figure 2. (a) Mean OTD lightning flash rate in June−August 1996−1999. (b) Mean GLD360 lightning stroke rate of June−August 2019−2021. (c) Same as panel b but counting only the lightning inside the TROPOMI swaths during the 3 h period before the TROPOMI overpass time. Grids with no lightning appear as the light-blue backgrounds in panels a−c. (d) Monthly ratio of panel c to panel b.

pressure detected by TROPOMI represents a pressure level inside the cloud rather than the geometrical cloud top.[65,66] It ranges from 130 to 987 hPa, with the most frequent values in the 250−300 hPa bin (Figure S3). The assumed LNO_2 profile should be more realistic than the default a priori NO_2 profile, because the high NO_2 is inside the cloud and the above-cloud NO_2 is low due to photolysis.[67] For high and thick clouds, the scattering weights are fairly uniform above the clouds, and the sensitivity of LNO_2 is highest around the middle of cloud, which is close to the cloud pressure detected by TROPOMI.[67] This minimizes the effects of possibly wrongly assumed NO_2 peak pressures on the retrieval.[68] Note that we find some cases with clouds higher than the tropopause. We dismiss these cases because the NO_2 concentration could be affected by stratospheric O_3.[28,69]

Estimation of the Lightning NO_2 Production Efficiency. As mentioned in NO2 Satellite Measurements, TROPOMI overpasses the same site north of 70° N several times. Thus, two consecutive orbits can observe the same thunderstorm. To make it easier to analyze patterns and variations in Arctic LNO_2 cases, we have created an interactive Web site (https://arctic-lightning-no2.streamlit.app/) that allows users to filter cases and investigate the relationship among LNO_2, cloud pressure, and lightning interactively.

The relationship between V_{LNO_2} (moles per square meter) at two timestamps can be defined as

$$\sum_{p_{(T_2)}} V_{LNO_{2_i}} A_i = e^{-(T_2-T_1)/\tau} \sum_{p_{(T_1)}} V_{LNO_{2_j}} A_j + PE \sum_{N} e^{-(T_2-t_k)/\tau} \quad (3)$$

where p is the number of pixels in the LNO_2 area, A is the area (square meters) of each pixel, T is the TROPOMI overpass time, t is the lightning occurrence time, τ is the near-convection LNO_2 lifetime, PE is the LNO_2 production efficiency (moles per stroke), and N is the total number of strokes during the interval between consecutive orbits. Specifically, the exponential component considers the chemical loss of NO_2. In eq 3, i and j are the pixel indices for the TROPOMI instrument, A_i and A_j are different LNO_2 areas taking advection into account (Figure S4), T_1 and T_2 represent the mean overpass times of the TROPOMI instrument over

https://doi.org/10.1021/acs.est.2c07988
Environ. Sci. Technol. XXXX, XXX, XXX−XXX

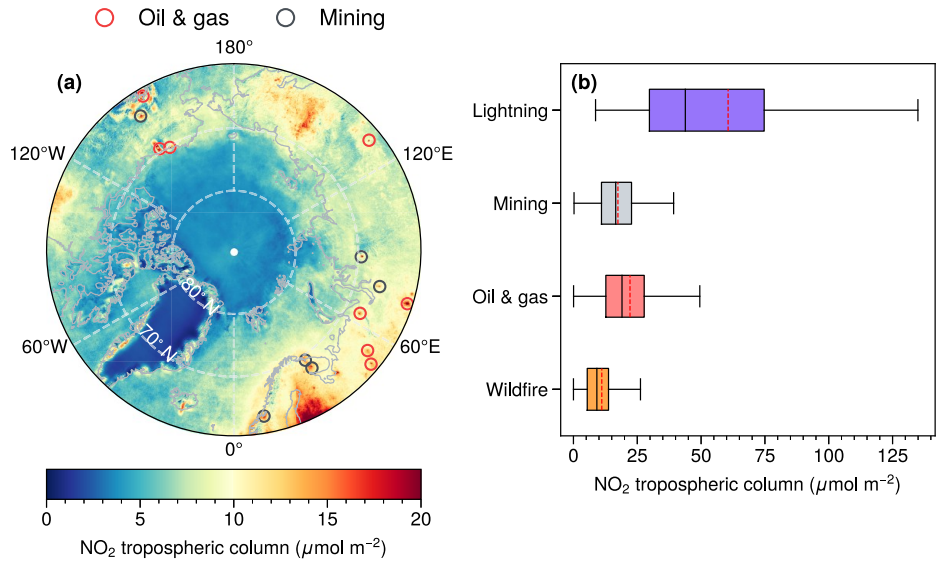

Figure 3. (a) Mean 4 km × 4 km TROPOMI tropospheric NO_2 column density in the local afternoon during June−August 2019−2021. The mining and oil and gas stations are shown as gray and red circles, respectively. (b) Comparisons of NO_2 among four sources: lightning, mining, oil and gas, and wildfire. The lightning bar represents the maximum NO_2 values over pixels for each lightning case, while the wildfire, mining, and oil and gas bars are the daily maximum NO_2 values at typical locations. The box plots indicate the median (black line) and mean (red line) values; the lower and upper boundaries represent the 25th and 75th percentiles, respectively, and the lower and upper error lines are the 10th and 90th percentiles, respectively.

the LNO_2 region for two consecutive orbits, and t_k represents the time of the kth lightning stroke (where k ranges from 1 to N) that occurs between the two orbits.

Note that if there is no lightning between two consecutive orbits, eq 3 can be simplified as

$$\sum_{p_{(T_2)}} V_{\mathrm{LNO}_{2_i}} A_i = \mathrm{e}^{-(T_2-T_1)/\tau} \sum_{p_{(T_1)}} V_{\mathrm{LNO}_{2_j}} A_j \quad (4)$$

We calculate the value of τ as 3 ± 1 h by analyzing the data from specific cases with high LNO_2 but no lightning between orbits (Table S2 and Figure S4). We then substitute the 3 h τ in eq 3 to calculate the LNO_2 PEs for the remaining lightning cases.

Previous studies have implemented three other methods to estimate LNO_2 production in tropical and mid-latitude regions, including (1) using linear regression to correlate background NO_2 plus LNO_2 (LNO_2*) with lightning,[39,70,71] (2) deriving LNO_2 directly using customized air mass factors,[28,67,72] and (3) deriving LNO_2* and subtracting background NO_2 derived from aircraft observations[70,73] or average NO_2 over non-lightning pixels.[38,40,56] However, the linear regression method is not suitable for our study due to variations in background NO_2 with solar zenith angle. The second approach requires detailed LNO_2 simulation with lightning parametrization, which is still quite uncertain,[13,14,16] particularly in the Arctic where lightning data are limited.[17] Additionally, obtaining mean background NO_2 data sets for each grid cell (i.e., 1° × 1°) in the Arctic is difficult, as TROPOMI detects only a few nonlightning convection cases north of 70° N (not shown).

RESULTS

Lightning Distributions. Figure 2 compares the spatial distribution of summer (June−August) lightning at high latitudes using satellite and ground-based lightning observations. Both data sets show higher rates over the Siberia and Alaska permafrost [60−65° N (Figure 2a,b)], which is the main Arctic fire regime.[74] The average OTD lightning flash rate and GLD360 stroke rate are 0.22 and 0.61 km^{-2} $month^{-1}$, respectively. However, OTD records less lightning near the Chukchi Sea and more over the Irminger Sea, which is likely due to interannual variations in Arctic precipitation linked to poleward moisture transport.[18]

To determine if LNO_2 can be detected by TROPOMI, we count the number of GLD360 lightning strokes within TROPOMI swaths during a 3 h period [i.e., the near-convection LNO_2 lifetime (see Estimation of the Lightning NO2 Production Efficiency)] before each overpass. TROPOMI does not continuously measure the Arctic, but it covers large parts of the region in summer with 14 overlapping orbits per day. The number of within-swath lightning strokes (Figure 2c) is ∼9% of the total counts and follows the same geographical pattern as the total strokes (Figure 2b). The proportion of within-swath lightning strokes increases with latitude from <10% (60−70° N) to 10−25% (70−80° N) and 40−100% [80−90° N (Figure 2d)] due to increased overlap of swaths at higher latitudes. Thus, the TROPOMI NO_2 observations are powerful for analyzing LNO_2 in the Arctic, where ground-based[75] and aircraft-based[76] NO_2 observations are limited. We choose to focus on the region north of 70° N for LNO_2 analysis due to the greater TROPOMI coverage and fewer NO_2 emissions from other sources (e.g., wildfires or gas production). The number of summer strokes detected by GLD360 is 1.2×10^6 (2019), 1.6×10^6 (2020), and 9.8×10^5 (2021) north of 70° N (Table S1). In the region with the highest TROPOMI coverage (80−90° N), the number of strokes in 2021 is $\sim 2.9 \times 10^4$, nearly twice as many as the total number recorded over the previous nine years.[77] The northernmost lightning stroke reaches 89.5° N, which was also reported (89.6° N) by the World Wide Lightning Location Network (WWLLN).[17]

Anthropogenic versus Lightning NO_2. Figure 3a shows the mean NO_2 column densities as measured by TROPOMI at high latitudes from June to August 2019−2021. While the

https://doi.org/10.1021/acs.est.2c07988
Environ. Sci. Technol. XXXX, XXX, XXX−XXX

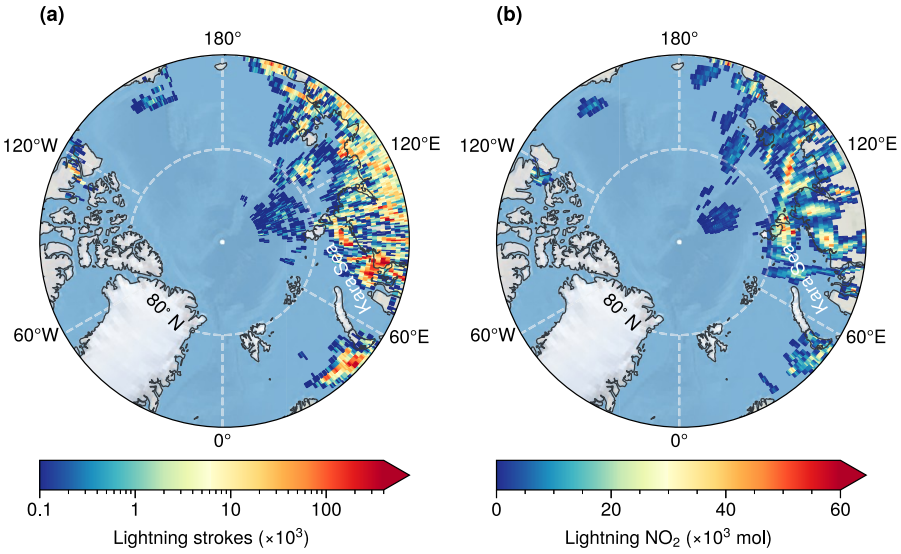

Figure 4. (a) Sum of GLD360 lightning strokes for selected cases per 0.5° × 0.5° grid. (b) Sum of lightning NO_2 derived from TROPOMI observations for selected cases per 0.5° × 0.5° grid.

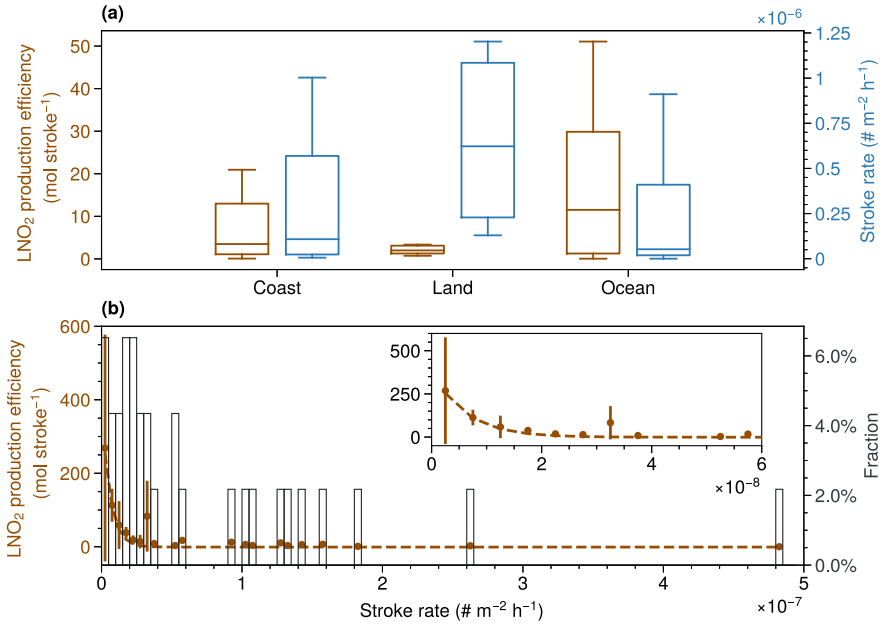

Figure 5. (a) Comparison of lightning NO_2 (LNO_2) production efficiency (brown) and stroke rate (blue) for three regions: coast, land, and ocean. The coast region is defined as a 500 m radius around the coastline. The box plots indicate the median values; the lower and upper boundaries represent the 25th and 75th percentiles, respectively, and the lower and upper error lines are the 10th and 90th percentiles, respectively. (b) LNO_2 production efficiency vs stroke rate, with histograms of case fractions in each 5 × 10^{-9} m^{-2} h^{-1} stroke rate bin overlaid.

averaged LNO_2 disappears into the background, NO_2 enhancements can still be observed over urban, industrial, and wildfire regions. For example, NO_2 correlated with mining operations (17 ± 2 μmol m^{-2}) in Alaska, Norway, and Russia is clearly visible. Other sources of NO_2 include oil and gas activities associated with the Mackenzie Valley in Arctic Canada, Prudhoe Bay/Kuparuk in North Alaska, and Yamal gas pipeline/Urengoy gas fields in Russia.[78] The NO_2 spikes along the Greenland coast may be false signals caused by retrieval complications due to the complicated topography of the region.[79] Contrary to NO_2 pollution, TROPOMI observations north of 70° N show low background NO_2 (4.4 ± 1.3 μmol m^{-2}), which is 45% lower than the mean NO_2 between 60° N and 65° N.

By comparing the highest LNO_2 column (61 ± 50 μmol m^{-2}) of all cases with typical anthropogenic and wildfire NO_2 at high latitudes (Figure 3b), we find that the median LNO_2 column density is triple, although the time scale of emission is on the order of hours. One particularly notable event is the deep convection occurring over the Laptev Sea (Figure S5), where the maximum LNO_2 is 246 μmol m^{-2}, comparable to the highest NO_2 column density (234 μmol m^{-2}) in the United States.[80] Given the significant contribution of LNO_2 for a few hours, it is important to calculate LNO_2 emissions in the Arctic.

Lightning NO_2 Production Efficiency and Emission. LNO_2 emission is the product of stroke counts and LNO_2 PEs (LNO_2 per stroke). It is impossible to derive the LNO_2 PE

https://doi.org/10.1021/acs.est.2c07988
Environ. Sci. Technol. XXXX, XXX, XXX−XXX

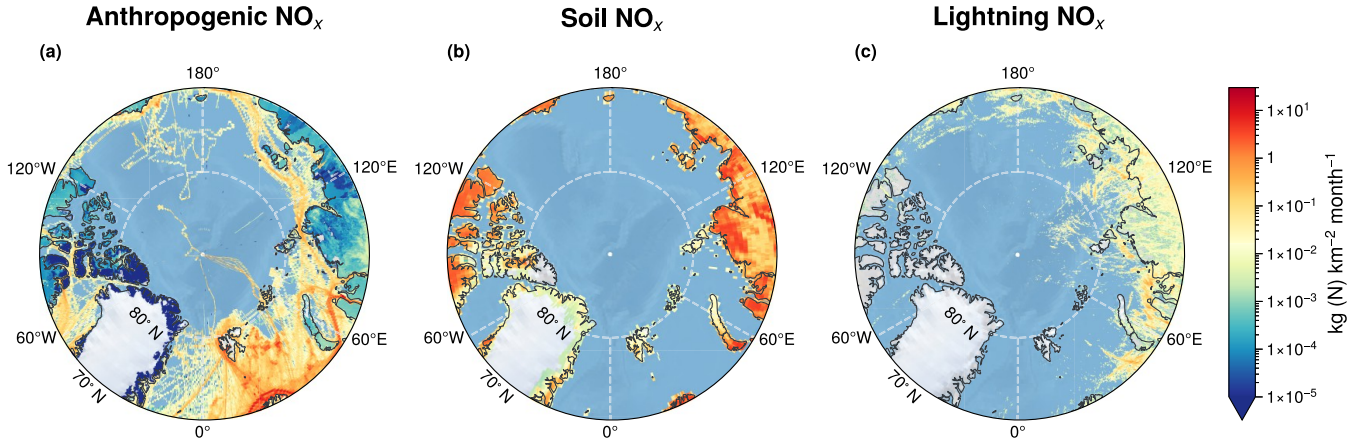

Figure 6. Monthly NO_x emissions in the Arctic from June to August. (a) Anthropogenic emissions including ship emissions, (b) soil emissions, and (c) lightning emissions. The lightning NO_x emissions are the mean values from 2019 to 2021, while the other emissions are from the 2018 Copernicus Atmosphere Monitoring Service (CAMS) global emission inventories.

directly on the basis of data from a single orbit, because the LNO_2 detected by TROPOMI includes both production and depletion, and a second orbit is needed for a time dimension. Here we utilize the LNO_2 from consecutive orbits to estimate the LNO_2 PEs (see Estimation of the Lightning NO2 Production Efficiency for details). On the basis of the screening of LNO_2 and lightning strokes, we choose 43 case studies with a total of 115 orbits. Cases between 60° W and 180° W are excluded due to insufficient LNO_2 or a lack of observations. Most cases are located between 60° E and 180° E (Figure 4a). By comparing the lightning distribution (Figure 4a) with the summed LNO_2 within a 0.5° × 0.5° grid box (Figure 4b), we find that the LNO_2 observed by TROPOMI has been transported away from the lightning source. For instance, although there is no lightning over the Kara Sea (77−80° N, 65−105° E), the LNO_2 in the region is ∼5.1×10^6 mol in total. This arises from the upper tropospheric wind transporting LNO_2 in the dominant downwind direction toward the east, highlighting the importance of matching lightning and NO_2.

Despite the transport of LNO_2, the comparison between the distribution of lightning and LNO_2 reveals a strong spatial correlation between the two phenomena. As a result, we estimate the LNO_2 PE for each case study. The median LNO_2 PEs are 2.0 (25th to 75th percentile, 1.3−3.1) mol $stroke^{-1}$, 3.5 (25th to 75th percentile, 1.1−13.0) mol $stroke^{-1}$, and 11.5 (25th to 75th percentile, 1.3−29.9) mol $stroke^{-1}$ over land, coast, and ocean, respectively (Figure 5a). In addition to these median values, we also measure the top 10 highest LNO_2 PEs, which range from 27 to 612 mol $stroke^{-1}$ (Table S3). These highest values are all found in oceanic or coastal areas. Due to the limited number of cases, it is not possible to determine if there is a statistically significant difference in LNO_2 PEs between ocean and land. However, the 2-fold larger LNO_2 PE in marine locations than in continents has also been found in the tropics and mid-latitudes[39,40,81] due to the higher flash energy of ocean-based lightning.[82,83]

Recent studies suggest that LNO_2 PE is related to flash size, with larger flashes producing more LNO_2.[36,81] Furthermore, stronger updrafts are associated with smaller flashes and higher lightning rates.[84−86] Therefore, we calculate the stroke rate, which is the number of lightning strokes per unit LNO_2 area per unit time. It ranges from 2.3×10^{-10} to 4.1×10^{-6} m^{-2} h^{-1}, with the continental stroke rate (6.2×10^{-7} m^{-2} h^{-1}) being ∼11 times higher than over the ocean (5.2×10^{-8} m^{-2} h^{-1}). We find an approximate power law relationship between the stroke rate and LNO_2 PE (Figure 5b). When the stroke rate decreases by 2 orders of magnitude, LNO_2 PE increases by a factor of 10, which is consistent with mid-latitude studies.[40,72]

Because the area applied in the stroke rate calculation depends on the LNO_2 selection from TROPOMI, we multiply the number of lightning strokes in each of the three regions by the median PEs of these regions and sum the results to obtain the total Arctic LNO_2 emissions [>70° N (Table S1)]. In 2020, LNO_2 emission is 109 Mg of N, which is 31% higher than the mean LNO_2 emission of 83 Mg of N in 2019 and 2021. The dominant contributor to this increase is the enhanced emission (35%) between 70° N and 80° N, where the mean convective available potential energy (CAPE) is 32% higher in 2020 (Table S1 and Figure S8). Note that LNO_2 emission (4.3 Mg of N) near the pole (80−90° N) increases by 353% in 2021 due to an increase in lightning activity (Table S1). Overall, we estimate the summer LNO_2 emission in the Arctic as 30 ± 16 Mg of N $month^{-1}$ considering the uncertainties [53% (Table S4)].

Assuming the ratio of NO_x to NO_2 as 2.4,[87] we estimate the LNO_x emission to be 73 Mg of N $month^{-1}$ and compare it with the anthropogenic and soil NO_x emissions in the Arctic during the summer (Figure 6). We find that soil emissions, totaling 2670 Mg of N $month^{-1}$, dominate NO_x over the Arctic land, while anthropogenic NO_x emissions of 350 Mg of N $month^{-1}$ over land are roughly the same in magnitude as wildfire emissions of 430 Mg of N $month^{-1}$. Ship emissions, totaling 1160 Mg of N $month^{-1}$, are the primary source of NO_x over the Arctic ocean. However, the LNO_x contributes 93% of NO_x in the northeastern region of the Arctic ocean (90−180° E, 80−90° N). It is important to note that the lifetime of upper tropospheric NO_2 away from thunderstorms is ∼0.5−8 days due to low temperatures;[20,23] therefore, further studies are needed to evaluate how LNO_2 affects O_3, CO, and CH_4 in the Arctic.

DISCUSSION

In this study, we estimate both the LNO_2 lifetime and the production efficiency in the Arctic based on consecutive TROPOMI NO_2 observations. Our results indicate that the 3

https://doi.org/10.1021/acs.est.2c07988
Environ. Sci. Technol. XXXX, XXX, XXX−XXX

h LNO_2 lifetime is similar to that previously reported in the United States.[23] The continental LNO_2 production efficiency [2.0 (1.3−3.1) mol stroke^{-1}] is also comparable to that observed over the United States (1.6 ± 0.1 mol stroke^{-1}).[71] Additionally, our findings suggest that oceanic lightning in the Arctic can produce 6 times higher NO_2 than continental lightning. As a result, when the amount of lightning increases by the same amount over the Arctic ocean and land, the oceanic lightning will produce more LNO_2. Overall, the mean LNO_x emissions (219 Mg of N) in summer (June−August) are equal to 5% of anthropogenic NO_x emissions in the Arctic.

One limitation of our study is that we derive the LNO_2 column density without retrieving LNO_2 vertical profiles. To obtain these profiles, techniques such as cloud slicing can be used,[88,89] but they require a large sample size to reduce noise. Future aircraft observations, like the Deep Convective Clouds and Chemistry (DC3) project,[90] could provide more detailed LNO_2 profiles and improve our understanding of LNO_x and air pollution in the Arctic.[75,91]

Accurate observations, simulations, and validations of Arctic lightning are crucial for understanding its impact on LNO_2 and other atmospheric processes, as global warming is expected to lead to an increase in its occurrence. However, the detection efficiency of ground-based lightning networks in the Arctic is still low due to the large areas of ocean and ice coverage in the region.[44] Additionally, current parametrizations of Arctic lightning tend to focus on land-based processes, particularly permafrost.[16] To address these challenges, consistent satellite observations, such as those provided by OTD, are essential. Note that the Lightning Imaging Sensors (LIS) on board the Tropical Rainfall Measuring Mission (TRMM)[92] and the International Space Station (ISS)[93] are primarily designed to detect tropical and mid-latitude lightning, with TRMM LIS covering low latitudes (±38°) and ISS LIS extending coverage to higher latitudes (up to ±55°). The range of latitudes that can be detected by future planned lightning sensors is currently unknown. However, carrying these sensors, such as the Geostationary Lightning Mapper (GLM) or the Lightning Mapping Instrument (LMI),[94,95] on hydrometeorological satellites like Arktika-M[96] could greatly benefit Arctic lightning studies by providing more comprehensive coverage of this region.

■ ASSOCIATED CONTENT

Data Availability Statement

The retrieval algorithm is available at https://github.com/zxdawn/S5P-LNO2.[97] The relevant data and analysis code are hosted at https://github.com/zxdawn/S5P-LNO2-Notebook.[98,99] We also established a Web site (https://arctic-lightning-no2.streamlit.app/) to provide an interactive interface for exploring Arctic lightning NO_2 cases. The data supporting the findings of this study are openly available: S5P-PAL TROPOMI data (https://data-portal.s5p-pal.com), NASA FIRMS VIIRS active fire product (https://earthdata.nasa.gov/firms), LIS/OTD 0.5 Degree High Resolution Monthly Climatology data set (10.5067/LIS/LIS-OTD/DATA303), ERA5 reanalysis data (10.24381/cds.bd0915c6), CAMS global emission inventories (https://ads.atmosphere.copernicus.eu/cdsapp#!/dataset/cams-global-emission-inventories), and global biomass burning emissions based on fire radiative power (GFAS, https://ads.atmosphere.copernicus.eu/cdsapp#!/dataset/cams-global-fire-emissions-gfas). The VAISALA GLD360 data are available upon request from VAISALA (https://www.vaisala.com/en/products/systems/lightning/gld360).

Supporting Information

The Supporting Information is available free of charge at https://pubs.acs.org/doi/10.1021/acs.est.2c07988.

Description of a priori lightning LNO_2 profiles; steps of selecting LNO_2 pixels; time series of GLD360 lightning strokes (Figure S2); histogram of TROPOMI cloud pressure and tropopause pressure (Figure S3); schematic overview of LNO_2 selections (Figure S4); large LNO_2 case (Figure S5); relationship between TROPOMI cloud pressure and above-cloud NO_2 column (Figure S6); time series of the flash rate recorded by the Optical Transient Detector (Figure S7); mean GLD360 lightning stroke rate, convective available potential energy, and aerosol optical depth (Figure S8); and tables describing the GLD360 stroke counts, LNO_2 lifetimes, LNO_2 production efficiencies, and uncertainties of LNO_2 estimations (PDF)

■ AUTHOR INFORMATION

Corresponding Authors

Xin Zhang − *KNMI-NUIST Center for Atmospheric Composition, Nanjing University of Information Science and Technology (NUIST), Nanjing 210044, China; Department of Satellite Observations, Royal Netherlands Meteorological Institute (KNMI), 3731 GA De Bilt, The Netherlands; Key Laboratory for Aerosol-Cloud-Precipitation of China Meteorological Administration, Nanjing University of Information Science and Technology (NUIST), Nanjing 210044, China;* orcid.org/0000-0002-1756-6620; Email: xinzhang1215@gmail.com

Yan Yin − *KNMI-NUIST Center for Atmospheric Composition, Nanjing University of Information Science and Technology (NUIST), Nanjing 210044, China; Key Laboratory for Aerosol-Cloud-Precipitation of China Meteorological Administration, Nanjing University of Information Science and Technology (NUIST), Nanjing 210044, China*; Email: yinyan@nuist.edu.cn

Authors

Ronald van der A − *KNMI-NUIST Center for Atmospheric Composition, Nanjing University of Information Science and Technology (NUIST), Nanjing 210044, China; Department of Satellite Observations, Royal Netherlands Meteorological Institute (KNMI), 3731 GA De Bilt, The Netherlands*

Jieying Ding − *Department of Satellite Observations, Royal Netherlands Meteorological Institute (KNMI), 3731 GA De Bilt, The Netherlands;* orcid.org/0000-0003-1263-2876

Henk Eskes − *Department of Satellite Observations, Royal Netherlands Meteorological Institute (KNMI), 3731 GA De Bilt, The Netherlands*

Jos van Geffen − *Department of Satellite Observations, Royal Netherlands Meteorological Institute (KNMI), 3731 GA De Bilt, The Netherlands;* orcid.org/0000-0003-2121-4553

Juliëtte Anema − *Department of Satellite Observations, Royal Netherlands Meteorological Institute (KNMI), 3731 GA De Bilt, The Netherlands; Wageningen University and Research, Meteorology and Air Quality, 6708 PB Wageningen, The Netherlands*

Chris Vagasky − *Vaisala Inc., Louisville, Colorado 80027, United States*

https://doi.org/10.1021/acs.est.2c07988
Environ. Sci. Technol. XXXX, XXX, XXX−XXX

Jeff L. Lapierre − *Earth Networks, Germantown, Maryland 20876, United States*
Xiang Kuang − *Key Laboratory for Aerosol-Cloud-Precipitation of China Meteorological Administration, Nanjing University of Information Science and Technology (NUIST), Nanjing 210044, China*

Complete contact information is available at: https://pubs.acs.org/10.1021/acs.est.2c07988

Notes

The authors declare no competing financial interest.

■ ACKNOWLEDGMENTS

This work was funded by the National Natural Science Foundation of China (Grants 91644224 and 42075176) and the China Scholarship Council (202009040001).

■ REFERENCES

(1) Reeve, N.; Toumi, R. Lightning Activity as an Indicator of Climate Change. *Q. J. R. Meteorol. Soc.* **1999**, *125*, 893−903.
(2) Williams, E. R. Lightning and Climate: A Review. *Atmos. Res.* **2005**, *76*, 272−287.
(3) Price, C. Will a Drier Climate Result in More Lightning? *Atmos. Res.* **2009**, *91*, 479−484.
(4) Price, C.; Rind, D. A Simple Lightning Parameterization for Calculating Global Lightning Distributions. *J. Geophys. Res. Atmos.* **1992**, *97*, 9919−9933.
(5) Price, C.; Penner, J.; Prather, M. NO_x from Lightning: 1. Global Distribution Based on Lightning Physics. *J. Geophys. Res. Atmos.* **1997**, *102*, 5929−5941.
(6) Allen, D. J.; Pickering, K. E. Evaluation of Lightning Flash Rate Parameterizations for Use in a Global Chemical Transport Model. *J. Geophys. Res.: Atmos.* **2002**, *107*, ACH 15-1−ACH 15-21.
(7) Futyan, J. M.; Del Genio, A. D. Relationships between Lightning and Properties of Convective Cloud Clusters. *Geophys. Res. Lett.* **2007**, *34*, L15705.
(8) Finney, D. L.; Doherty, R. M.; Wild, O.; Huntrieser, H.; Pumphrey, H. C.; Blyth, A. M. Using Cloud Ice Flux to Parametrise Large-Scale Lightning. *Atmos. Chem. Phys.* **2014**, *14*, 12665−12682.
(9) Romps, D. M.; Seeley, J. T.; Vollaro; Molinari, J. Projected Increase in Lightning Strikes in the United States Due to Global Warming. *Science* **2014**, *346*, 851−854.
(10) Price, C.; Rind, D. Modeling Global Lightning Distributions in a General Circulation Model. *Mon. Wea. Rev.* **1994**, *122*, 1930−1939.
(11) Michalon, N.; Nassif, A.; Saouri, T.; Royer, J. F.; Pontikis, C. A. Contribution to the Climatological Study of Lightning. *Geophys. Res. Lett.* **1999**, *26*, 3097−3100.
(12) Luhar, A. K.; Galbally, I. E.; Woodhouse, M. T.; Abraham, N. L. Assessing and Improving Cloud-Height-Based Parameterisations of Global Lightning Flash Rate, and Their Impact on Lightning-Produced NO_x and Tropospheric Composition in a Chemistry-Climate Model. *Atmos. Chem. Phys.* **2021**, *21*, 7053−7082.
(13) Finney, D. L.; Doherty, R. M.; Wild, O.; Stevenson, D. S.; MacKenzie, I. A.; Blyth, A. M. A Projected Decrease in Lightning under Climate Change. *Nat. Clim. Chang.* **2018**, *8*, 210−213.
(14) Romps, D. M. Evaluating the Future of Lightning in Cloud-resolving Models. *Geophys. Res. Lett.* **2019**, *46*, 14863−14871.
(15) Rantanen, M.; Karpechko, A. Y.; Lipponen, A.; Nordling, K.; Hyvärinen, O.; Ruosteenoja, K.; Vihma, T.; Laaksonen, A. The Arctic Has Warmed Nearly Four Times Faster than the Globe since 1979. *Communications Earth & Environment* **2022**, *3*, 1−10.
(16) Chen, Y.; Romps, D. M.; Seeley, J. T.; Veraverbeke, S.; Riley, W. J.; Mekonnen, Z. A.; Randerson, J. T. Future Increases in Arctic Lightning and Fire Risk for Permafrost Carbon. *Nat. Clim. Chang.* **2021**, *11*, 404−410.
(17) Holzworth, R. H.; Brundell, J. B.; McCarthy, M. P.; Jacobson, A. R.; Rodger, C. J.; Anderson, T. S. Lightning in the Arctic. *Geophys. Res. Lett.* **2021**, *48*, e2020GL091366.
(18) Bintanja, R.; van der Wiel, K.; van der Linden, E. C.; Reusen, J.; Bogerd, L.; Krikken, F.; Selten, F. M. Strong Future Increases in Arctic Precipitation Variability Linked to Poleward Moisture Transport. *Sci. Adv.* **2020**, *6*, eaax6869.
(19) Zel'dovich, Y.; Raizer, Y. In *Physics of Shock Waves and High-Temperature Hydrodynamic Phenomena*; Hayes, W. D., Probstein, R. F., Zel'dovich, Y., Raizer, Y., Eds.; Academic Press, 1967; pp 566−571.
(20) Schumann, U.; Huntrieser, H. The Global Lightning-Induced Nitrogen Oxides Source. *Atmos. Chem. Phys.* **2007**, *7*, 3823−3907.
(21) Jaeglé, L.; Jacob, D. J.; Wang, Y.; Weinheimer, A. J.; Ridley, B. A.; Campos, T. L.; Sachse, G. W.; Hagen, D. E. Sources and Chemistry of NO_x in the Upper Troposphere over the United States. *Geophys. Res. Lett.* **1998**, *25*, 1705−1708.
(22) Martin, R. V.; Sauvage, B.; Folkins, I.; Sioris, C. E.; Boone, C.; Bernath, P.; Ziemke, J. Space-Based Constraints on the Production of Nitric Oxide by Lightning. *J. Geophys. Res.: Atmos.* **2007**, *112*, 1479.
(23) Nault, B. A.; Laughner, J. L.; Wooldridge, P. J.; Crounse, J. D.; Dibb, J.; Diskin, G.; Peischl, J.; Podolske, J. R.; Pollack, I. B.; Ryerson, T. B.; Scheuer, E.; Wennberg, P. O.; Cohen, R. C. Lightning NO_x Emissions: Reconciling Measured and Modeled Estimates With Updated NO_x Chemistry. *Geophys. Res. Lett.* **2017**, *44*, 9479−9488.
(24) Pickering, K. E.; Thompson, A. M.; Tao, W.-K.; Kucsera, T. L. Upper Tropospheric Ozone Production Following Mesoscale Convection during STEP/EMEX. *J. Geophys. Res. Atmos.* **1993**, *98*, 8737−8749.
(25) Pickering, K. E.; Thompson, A. M.; Wang, Y.; Tao, W.-K.; McNamara, D. P.; Kirchhoff, V. W. J. H.; Heikes, B. G.; Sachse, G. W.; Bradshaw, J. D.; Gregory, G. L.; Blake, D. R. Convective Transport of Biomass Burning Emissions over Brazil during TRACE A. *J. Geophys. Res. Atmos.* **1996**, *101*, 23993−24012.
(26) Kang, D.; Mathur, R.; Pouliot, G. A.; Gilliam, R. C.; Wong, D. C. Significant Ground-Level Ozone Attributed to Lightning-Induced Nitrogen Oxides during Summertime over the Mountain West States. *npj Clim. Atmos. Sci.* **2020**, *3*, 6.
(27) Iglesias-Suarez, F.; Kinnison, D. E.; Rap, A.; Maycock, A. C.; Wild, O.; Young, P. J. Key Drivers of Ozone Change and Its Radiative Forcing over the 21st Century. *Atmos. Chem. Phys.* **2018**, *18*, 6121−6139.
(28) Zhang, X.; Yin, Y.; van der A, R.; Eskes, H.; van Geffen, J.; Li, Y.; Kuang, X.; Lapierre, J. L.; Chen, K.; Zhen, Z.; Hu, J.; He, C.; Chen, J.; Shi, R.; Zhang, J.; Ye, X.; Chen, H. Influence of Convection on the Upper-Tropospheric O_3 and NO_x Budget in Southeastern China. *Atmos. Chem. Phys.* **2022**, *22*, 5925−5942.
(29) Labrador, L. J.; von Kuhlmann, R.; Lawrence, M. G. Strong Sensitivity of the Global Mean OH Concentration and the Tropospheric Oxidizing Efficiency to the Source of NO_x from Lightning. *Geophys. Res. Lett.* **2004**, *31*, L06102.
(30) Brune, W. H.; McFarland, P. J.; Bruning, E.; Waugh, S.; MacGorman, D.; Miller, D. O.; Jenkins, J. M.; Ren, X.; Mao, J.; Peischl, J. Extreme Oxidant Amounts Produced by Lightning in Storm Clouds. *Science* **2021**, *372*, 711−715.
(31) Jenkins, J. M.; Brune, W. H.; Miller, D. O. Electrical Discharges Produce Prodigious Amounts of Hydroxyl and Hydroperoxyl Radicals. *J. Geophys. Res.: Atmos.* **2021**, *126*, e2021JD034557.
(32) Mao, J.; Zhao, T.; Keller, C. A.; Wang, X.; McFarland, P. J.; Jenkins, J. M.; Brune, W. H. Global Impact of Lightning-Produced Oxidants. *Geophys. Res. Lett.* **2021**, *48*, e2021GL095740.
(33) Fiore, A. M.; Horowitz, L. W.; Dlugokencky, E. J.; West, J. J. Impact of Meteorology and Emissions on Methane Trends, 1990−2004. *Geophys. Res. Lett.* **2006**, *33*, L12809.
(34) Murray, L. T. Lightning NO_x and Impacts on Air Quality. *Curr. Pollution. Rep.* **2016**, *2*, 115−133.
(35) He, J.; Loboda, T. V.; Chen, D.; French, N. H. F. Cloud-to-Ground Lightning and Near-Surface Fire Weather Control Wildfire

Occurrence in Arctic Tundra. *Geophys. Res. Lett.* **2022**, *49*, e2021GL096814.
(36) Huntrieser, H.; Schumann, U.; Schlager, H.; Höller, H.; Giez, A.; Betz, H.-D.; Brunner, D.; Forster, C.; Pinto, O.; Calheiros, R. Lightning Activity in Brazilian Thunderstorms during TROCCINOX: Implications for NO_x Production. *Atmos. Chem. Phys.* **2008**, *8*, 921−953.
(37) Beirle, S.; Huntrieser, H.; Wagner, T. Direct Satellite Observation of Lightning-Produced NO_x. *Atmos. Chem. Phys.* **2010**, *10*, 10965−10986.
(38) Bucsela, E. J.; Pickering, K. E.; Huntemann, T. L.; Cohen, R. C.; Perring, A.; Gleason, J. F.; Blakeslee, R. J.; Albrecht, R. I.; Holzworth, R.; Cipriani, J. P.; Vargas-Navarro, D.; Mora-Segura, I.; Pacheco-Hernández, A.; Laporte-Molina, S. Lightning-Generated NO_x Seen by the Ozone Monitoring Instrument during NASA's Tropical Composition, Cloud and Climate Coupling Experiment (TC4). *J. Geophys. Res.: Atmos.* **2010**, *115*, 793.
(39) Allen, D. J.; Pickering, K. E.; Bucsela, E.; Krotkov, N.; Holzworth, R. Lightning NO_x Production in the Tropics as Determined Using OMI NO_2 Retrievals and WWLLN Stroke Data. *J. Geophys. Res. Atmos.* **2019**, *124*, 13498−13518.
(40) Bucsela, E. J.; Pickering, K. E.; Allen, D.; Holzworth, R.; Krotkov, N. Midlatitude Lightning NO_x Production Efficiency Inferred from OMI and WWLLN Data. *J. Geophys. Res. Atmos.* **2019**, *124*, 13475−13497.
(41) Said, R. K.; Inan, U. S.; Cummins, K. L. Long-Range Lightning Geolocation Using a VLF Radio Atmospheric Waveform Bank. *J. Geophys. Res.: Atmos.* **2010**, *115*, D23108.
(42) Said, R. K.; Cohen, M. B.; Inan, U. S. Highly Intense Lightning over the Oceans: Estimated Peak Currents from Global GLD360 Observations. *J. Geophys. Res. Atmos.* **2013**, *118*, 6905−6915.
(43) Said, R. Towards a Global Lightning Locating System. *Weather* **2017**, *72*, 36−40.
(44) Vagasky, C. A.*Trends in Lightning in the Arctic Region Using GLD360. Collective Madison Meeting*; 2022.
(45) Schulz, W.; Cummins, K.; Diendorfer, G.; Dorninger, M. Cloud-to-Ground Lightning in Austria: A 10-Year Study Using Data from a Lightning Location System. *J. Geophys. Res.: Atmos.* **2005**, *110*, D09101.
(46) Yair, Y.; Shalev, S.; Erlich, Z.; Agrachov, A.; Katz, E.; Saaroni, H.; Price, C.; Ziv, B. Lightning Flash Multiplicity in Eastern Mediterranean Thunderstorms. *Nat. Hazards Earth Syst. Sci.* **2014**, *14*, 165−173.
(47) Bürgesser, R. E. Assessment of the World Wide Lightning Location Network (WWLLN) Detection Efficiency by Comparison to the Lightning Imaging Sensor (LIS). *Q. J. R. Meteorol. Soc.* **2017**, *143*, 2809−2817.
(48) Kolmašová, I.; Santolík, O.; Rosická, K. Lightning Activity in Northern Europe during a Stormy Winter: Disruptions of Weather Patterns Originating in Global Climate Phenomena. *Atmos. Chem. Phys.* **2022**, *22*, 3379−3389.
(49) Yusop, N.; Ahmad, M. R.; Abdullah, M.; Zainudin, S. K.; Nor, W. N. A. W. M.; Alhasa, K. M.; Esa, M. R. M.; Sabri, M. H. M.; Suparta, W.; Gulisano, A. M.; Cooray, V. Cloud-to-Ground Lightning Observations over the Western Antarctic Region. *Polar Sci.* **2019**, *20*, 84−91.
(50) Mackerras, D.; Darveniza, M. Latitudinal Variation of Lightning Occurrence Characteristics. *J. Geophys. Res. Atmos.* **1994**, *99*, 10813−10821.
(51) Prentice, S. A.; Mackerras, D. The Ratio of Cloud to Cloud-Ground Lightning Flashes in Thunderstorms. *J. Appl. Meteorol. Climatol.* **1977**, *16*, 545−550.
(52) Bandholnopparat, K.; Sato, M.; Adachi, T.; Ushio, T.; Takahashi, Y. Estimation of the IC to CG Ratio Using JEM-GLIMS and Ground-Based Lightning Network Data. *J. Geophys. Res.: Atmos.* **2020**, *125*, e2019JD032195.
(53) Christian, H. J.; Blakeslee, R. J.; Boccippio, D. J.; Boeck, W. L.; Buechler, D. E.; Driscoll, K. T.; Goodman, S. J.; Hall, J. M.; Koshak, W. J.; Mach, D. M.; Stewart, M. F. Global Frequency and Distribution of Lightning as Observed from Space by the Optical Transient Detector. *J. Geophys. Res.: Atmos.* **2003**, *108*, ACL 4-1−ACL 4-15.
(54) Veefkind, J. P.; Aben, I.; McMullan, K.; Förster, H.; de Vries, J.; Otter, G.; Claas, J.; Eskes, H. J.; de Haan, J. F.; Kleipool, Q.; van Weele, M.; Hasekamp, O.; Hoogeveen, R.; Landgraf, J.; Snel, R.; Tol, P.; Ingmann, P.; Voors, R.; Kruizinga, B.; Vink, R.; Visser, H.; Levelt, P. F. TROPOMI on the ESA Sentinel-5 Precursor: A GMES Mission for Global Observations of the Atmospheric Composition for Climate, Air Quality and Ozone Layer Applications. *Remote Sensing of Environment* **2012**, *120*, 70−83.
(55) van Geffen, J.; Eskes, H.; Compernolle, S.; Pinardi, G.; Verhoelst, T.; Lambert, J.-C.; Sneep, M.; ter Linden, M.; Ludewig, A.; Boersma, K. F.; Veefkind, J. P. Sentinel-5P TROPOMI NO_2 Retrieval: Impact of Version v2.2 Improvements and Comparisons with OMI and Ground-Based Data. *Atmos. Meas. Technol.* **2022**, *15*, 2037−2060.
(56) Allen, D. J.; Pickering, K. E.; Bucsela, E.; Van Geffen, J.; Lapierre, J.; Koshak, W.; Eskes, H. Observations of Lightning NO_x Production from TROPOMI Case Studies over the United States. *J. Geophys. Res.: Atmos.* **2021**, *126*, e2020JD034174.
(57) Bäcklund, H.; Hedblom, A.; Neijman, N. A Density-Based Spatial Clustering of Application with Noise. *Data Mining TNM033* **2011**, 11−30.
(58) Schubert, E.; Sander, J.; Ester, M.; Kriegel, H. P.; Xu, X. DBSCAN Revisited, Revisited: Why and How You Should (Still) Use DBSCAN. *ACM Trans. Database Syst.* **2017**, *42*, 1−21.
(59) Hersbach, H.; Bell, B.; Berrisford, P.; Hirahara, S.; Horányi, A.; Muñoz-Sabater, J.; Nicolas, J.; Peubey, C.; Radu, R.; Schepers, D.; Simmons, A.; Soci, C.; Abdalla, S.; Abellan, X.; Balsamo, G.; Bechtold, P.; Biavati, G.; Bidlot, J.; Bonavita, M.; Chiara, G.; Dahlgren, P.; Dee, D.; Diamantakis, M.; Dragani, R.; Flemming, J.; Forbes, R.; Fuentes, M.; Geer, A.; Haimberger, L.; Healy, S.; Hogan, R. J.; Hólm, E.; Janisková, M.; Keeley, S.; Laloyaux, P.; Lopez, P.; Lupu, C.; Radnoti, G.; Rosnay, P.; Rozum, I.; Vamborg, F.; Villaume, S.; Thépaut, J.-N. The ERA5 Global Reanalysis. *Q. J. R. Meteorol. Soc.* **2020**, *146*, 1999−2049.
(60) Soille, P. J.; Ansoult, M. M. Automated Basin Delineation from Digital Elevation Models Using Mathematical Morphology. *Signal Process.* **1990**, *20*, 171−182.
(61) Heikenfeld, M.; Marinescu, P. J.; Christensen, M.; Watson-Parris, D.; Senf, F.; van den Heever, S. C.; Stier, P. Tobac 1.2: Towards a Flexible Framework for Tracking and Analysis of Clouds in Diverse Datasets. *Geosci. Model Dev.* **2019**, *12*, 4551−4570.
(62) Lorente, A.; Folkert Boersma, K.; Yu, H.; Dörner, S.; Hilboll, A.; Richter, A.; Liu, M.; Lamsal, L. N.; Barkley, M.; De Smedt, I.; van Roozendael, M.; Wang, Y.; Wagner, T.; Beirle, S.; Lin, J.-T.; Krotkov, N.; Stammes, P.; Wang, P.; Eskes, H. J.; Krol, M. Structural Uncertainty in Air Mass Factor Calculation for NO_2 and HCHO Satellite Retrievals. *Atmos. Meas. Tech.* **2017**, *10*, 759−782.
(63) Ott, L. E.; Pickering, K. E.; Stenchikov, G. L.; Allen, D. J.; DeCaria, A. J.; Ridley, B.; Lin, R.-F.; Lang, S.; Tao, W.-K. Production of Lightning NO_x and Its Vertical Distribution Calculated from Three-Dimensional Cloud-Scale Chemical Transport Model Simulations. *J. Geophys. Res.: Atmos.* **2010**, *115*, 4711.
(64) Luo, C.; Wang, Y.; Koshak, W. J. Development of a Self-Consistent Lightning NO_x Simulation in Large-Scale 3-D Models. *J. Geophys. Res. Atmos.* **2017**, *122*, 3141−3154.
(65) Vasilkov, A.; Joiner, J.; Spurr, R.; Bhartia, P. K.; Levelt, P.; Stephens, G. Evaluation of the OMI Cloud Pressures Derived from Rotational Raman Scattering by Comparisons with Other Satellite Data and Radiative Transfer Simulations. *J. Geophys. Res.: Atmos.* **2008**, *113*, D15S19.
(66) Joiner, J.; Vasilkov, A. P.; Gupta, P.; Bhartia, P. K.; Veefkind, P.; Sneep, M.; de Haan, J.; Polonsky, I.; Spurr, R. Fast Simulators for Satellite Cloud Optical Centroid Pressure Retrievals; Evaluation of OMI Cloud Retrievals. *Atmos. Meas. Tech.* **2012**, *5*, 529−545.
(67) Beirle, S.; Salzmann, M.; Lawrence, M. G.; Wagner, T. Sensitivity of Satellite Observations for Freshly Produced Lightning NO_x. *Atmos. Chem. Phys.* **2009**, *9*, 1077−1094.

https://doi.org/10.1021/acs.est.2c07988
Environ. Sci. Technol. XXXX, XXX, XXX−XXX

(68) Laughner, J. L.; Cohen, R. C. Quantification of the Effect of Modeled Lightning NO_2 on UV-Visible Air Mass Factors. *Atmos. Meas. Technol.* **2017**, *10*, 4403−4419.
(69) Frey, W.; Schofield, R.; Hoor, P.; Kunkel, D.; Ravegnani, F.; Ulanovsky, A.; Viciani, S.; D'Amato, F.; Lane, T. P. The Impact of Overshooting Deep Convection on Local Transport and Mixing in the Tropical Upper Troposphere/Lower Stratosphere (UTLS). *Atmos. Chem. Phys.* **2015**, *15*, 6467−6486.
(70) Pickering, K. E.; Bucsela, E.; Allen, D.; Ring, A.; Holzworth, R.; Krotkov, N. Estimates of Lightning NO_x Production Based on OMI NO_2 Observations over the Gulf of Mexico. *J. Geophys. Res. Atmos.* **2016**, *121*, 8668−8691.
(71) Lapierre, J. L.; Laughner, J. L.; Geddes, J. A.; Koshak, W.; Cohen, R. C.; Pusede, S. E. Observing U.S. Regional Variability in Lightning NO_2 Production Rates. *J. Geophys. Res.: Atmos.* **2020**, *125*, e2019JD031362.
(72) Zhang, X.; Yin, Y.; van der A, R.; Lapierre, J. L.; Chen, Q.; Kuang, X.; Yan, S.; Chen, J.; He, C.; Shi, R. Estimates of Lightning NO_x Production Based on High-Resolution OMI NO_2 Retrievals over the Continental US. *Atmos. Meas. Tech.* **2020**, *13*, 1709−1734.
(73) Pérez-Invernón, F. J.; Huntrieser, H.; Erbertseder, T.; Loyola, D.; Valks, P.; Liu, S.; Allen, D. J.; Pickering, K. E.; Bucsela, E. J.; Jöckel, P.; van Geffen, J.; Eskes, H.; Soler, S.; Gordillo-Vázquez, F. J.; Lapierre, J. Quantification of Lightning-Produced NO_x over the Pyrenees and the Ebro Valley by Using Different TROPOMI-NO_2 and Cloud Research Products. *Atmos. Meas. Technol.* **2022**, *15*, 3329−3351.
(74) McCarty, J. L.; Aalto, J.; Paunu, V.-V.; Arnold, S. R.; Eckhardt, S.; Klimont, Z.; Fain, J. J.; Evangeliou, N.; Venäläinen, A.; Tchebakova, N. M.; Parfenova, E. I.; Kupiainen, K.; Soja, A. J.; Huang, L.; Wilson, S. Reviews and Syntheses: Arctic Fire Regimes and Emissions in the 21st Century. *Biogeosciences* **2021**, *18*, 5053−5083.
(75) Schmale, J.; Arnold, S. R.; Law, K. S.; Thorp, T.; Anenberg, S.; Simpson, W. R.; Mao, J.; Pratt, K. A. Local Arctic Air Pollution: A Neglected but Serious Problem. *Earth's Future* **2018**, *6*, 1385−1412.
(76) Jacob, D. J.; Crawford, J. H.; Maring, H.; Clarke, A. D.; Dibb, J. E.; Emmons, L. K.; Ferrare, R. A.; Hostetler, C. A.; Russell, P. B.; Singh, H. B.; Thompson, A. M.; Shaw, G. E.; McCauley, E.; Pederson, J. R.; Fisher, J. A. The Arctic Research of the Composition of the Troposphere from Aircraft and Satellites (ARCTAS) Mission: Design, Execution, and First Results. *Atmos. Chem. Phys.* **2010**, *10*, 5191−5212.
(77) Network, V. L. D.Total Lightning Statistics 2021: Vaisala Annual Lightning Report. 2021.
(78) van der A, R. J.; de Laat, A. T. J.; Ding, J.; Eskes, H. J. Connecting the Dots: NO_x Emissions along a West Siberian Natural Gas Pipeline. *npj Clim. Atmos. Sci.* **2020**, *3*, 16.
(79) Hachmeister, J.; Schneising, O.; Buchwitz, M.; Lorente, A.; Borsdorff, T.; Burrows, J. P.; Notholt, J.; Buschmann, M. On the Influence of Underlying Elevation Data on Sentinel-5 Precursor TROPOMI Satellite Methane Retrievals over Greenland. *Atmos. Meas. Technol.* **2022**, *15*, 4063−4074.
(80) Goldberg, D. L.; Anenberg, S. C.; Kerr, G. H.; Mohegh, A.; Lu, Z.; Streets, D. G. TROPOMI NO_2 in the United States: A Detailed Look at the Annual Averages, Weekly Cycles, Effects of Temperature, and Correlation With Surface NO_2 Concentrations. *Earth's Future* **2021**, *9*, e2020EF001665.
(81) Marais, E. A.; Jacob, D. J.; Choi, S.; Joiner, J.; Belmonte-Rivas, M.; Cohen, R. C.; Beirle, S.; Murray, L. T.; Schiferl, L. D.; Shah, V.; Jaeglé, L. Nitrogen Oxides in the Global Upper Troposphere: Interpreting Cloud-Sliced NO_2 Observations from the OMI Satellite Instrument. *Atmos. Chem. Phys.* **2018**, *18*, 17017−17027.
(82) Beirle, S.; Koshak, W.; Blakeslee, R.; Wagner, T. Global Patterns of Lightning Properties Derived by OTD and LIS. *Nat. Hazards Earth Syst. Sci.* **2014**, *14*, 2715−2726.
(83) Hutchins, M. L.; Holzworth, R. H.; Virts, K. S.; Wallace, J. M.; Heckman, S. Radiated VLF Energy Differences of Land and Oceanic Lightning. *Geophys. Res. Lett.* **2013**, *40*, 2390−2394.
(84) Bruning, E. C.; MacGorman, D. R. Theory and Observations of Controls on Lightning Flash Size Spectra. *J. Atmos. Sci.* **2013**, *70*, 4012−4029.
(85) Bruning, E. C.; Thomas, R. J. Lightning Channel Length and Flash Energy Determined from Moments of the Flash Area Distribution. *J. Geophys. Res. Atmos.* **2015**, *120*, 8925−8940.
(86) Mecikalski, R. M.; Bain, A. L.; Carey, L. D. Radar and Lightning Observations of Deep Moist Convection across Northern Alabama during DC3:21 May 2012. *Mon. Wea. Rev.* **2015**, *143*, 2774−2794.
(87) Silvern, R. F.; Jacob, D. J.; Travis, K. R.; Sherwen, T.; Evans, M. J.; Cohen, R. C.; Laughner, J. L.; Hall, S. R.; Ullmann, K.; Crounse, J. D.; Wennberg, P. O.; Peischl, J.; Pollack, I. B. Observed NO/NO_2 Ratios in the Upper Troposphere Imply Errors in NO-NO_2-O_3 Cycling Kinetics or an Unaccounted NO_x Reservoir. *Geophys. Res. Lett.* **2018**, *45*, 4466−4474.
(88) Belmonte Rivas, M.; Veefkind, P.; Eskes, H.; Levelt, P. OMI Tropospheric NO_2 Profiles from Cloud Slicing: Constraints on Surface Emissions, Convective Transport and Lightning NO_x. *Atmos. Chem. Phys.* **2015**, *15*, 13519−13553.
(89) Marais, E. A.; Roberts, J. F.; Ryan, R. G.; Eskes, H.; Boersma, K. F.; Choi, S.; Joiner, J.; Abuhassan, N.; Redondas, A.; Grutter, M.; Cede, A.; Gomez, L.; Navarro-Comas, M. New Observations of NO_2 in the Upper Troposphere from TROPOMI. *Atmos. Meas. Technol.* **2021**, *14*, 2389−2408.
(90) Barth, M. C.; Rutledge, S. A.; Brune, W. H.; Cantrell, C. A. Introduction to the Deep Convective Clouds and Chemistry (DC3) 2012 Studies. *J. Geophys. Res. Atmos.* **2019**, *124*, 8095−8103.
(91) Law, K. S.; Stohl, A. Arctic Air Pollution: Origins and Impacts. *Science* **2007**, *315*, 1537−1540.
(92) Cecil, D. J.; Buechler, D. E.; Blakeslee, R. J. Gridded Lightning Climatology from TRMM-LIS and OTD: Dataset Description. *Atmos. Res.* **2014**, *135*−*136*, 404−414.
(93) Blakeslee, R. J.; Lang, T. J.; Koshak, W. J.; Buechler, D.; Gatlin, P.; Mach, D. M.; Stano, G. T.; Virts, K. S.; Walker, T. D.; Cecil, D. J.; Ellett, W.; Goodman, S. J.; Harrison, S.; Hawkins, D. L.; Heumesser, M.; Lin, H.; Maskey, M.; Schultz, C. J.; Stewart, M.; Bateman, M.; Chanrion, O.; Christian, H. Three Years of the Lightning Imaging Sensor Onboard the International Space Station: Expanded Global Coverage and Enhanced Applications. *J. Geophys. Res.: Atmos.* **2020**, *125*, e2020JD032918.
(94) Goodman, S. J.; Blakeslee, R. J.; Koshak, W. J.; Mach, D.; Bailey, J.; Buechler, D.; Carey, L.; Schultz, C.; Bateman, M.; McCaul, E.; Stano, G. The GOES-R Geostationary Lightning Mapper (GLM). *Atmos. Res.* **2013**, *125*−*126*, 34−49.
(95) Yang, J.; Zhang, Z.; Wei, C.; Lu, F.; Guo, Q. Introducing the New Generation of Chinese Geostationary Weather Satellites, Fengyun-4. *Bull. Am. Meteor. Soc.* **2017**, *98*, 1637−1658.
(96) Asmus, V. V.; Milekhin, O. E.; Kramareva, L. S.; Khailov, M. N.; Shirshakov, A. E.; Shumakov, I. A. Arktika-M: The World's First Highly Elliptical Orbit Hydrometeorological Space System. *Russ. Meteorol. Hydrol.* **2021**, *46*, 805−816.
(97) Zhang, X.*Zxdawn/S5P-LNO2*, ver. 1.0; Zenodo, 2023.
(98) Zhang, X.*Zxdawn/S5P-LNO2-Notebook*, ver. 1.0; Zenodo, 2023.
(99) Zhang, X. Data set for Spaceborne Observations of Lightning NO_2 in the Arctic. 2023.

https://doi.org/10.1021/acs.est.2c07988
Environ. Sci. Technol. XXXX, XXX, XXX−XXX